ARTICLE

# Mutations in *ATP6V1E1* or *ATP6V1A* Cause Autosomal-Recessive Cutis Laxa

Tim Van Damme,[1,25] Thatjana Gardeitchik,[2,3,25] Miski Mohamed,[2,25] Sergio Guerrero-Castillo,[4,5,26] Peter Freisinger,[6,26] Brecht Guillemyn,[1,26] Ariana Kariminejad,[7,26] Daisy Dalloyaux,[2,5] Sanne van Kraaij,[2,5] Dirk J. Lefeber,[5,8] Delfien Syx,[1] Wouter Steyaert,[1] Riet De Rycke,[9,10] Alexander Hoischen,[3] Erik-Jan Kamsteeg,[3] Sunnie Y. Wong,[11] Monique van Scherpenzeel,[5,8] Payman Jamali,[12] Ulrich Brandt,[4,5] Leo Nijtmans,[4,5] G. Christoph Korenke,[13] Brian H.Y. Chung,[14] Christopher C.Y. Mak,[14] Ingrid Hausser,[15] Uwe Kornak,[16,17] Björn Fischer-Zirnsak,[16,17] Tim M. Strom,[18] Thomas Meitinger,[18] Yasemin Alanay,[19] Gulen E. Utine,[20] Peter K.C. Leung,[14] Siavash Ghaderi-Sohi,[7] Paul Coucke,[1] Sofie Symoens,[1] Anne De Paepe,[1] Christian Thiel,[21] Tobias B. Haack,[18,22,23] Fransiska Malfait,[1,27] Eva Morava,[11,24,27] Bert Callewaert,[1,27,*] and Ron A. Wevers[5,27,*]

Defects of the V-type proton ($H^+$) ATPase (V-ATPase) impair acidification and intracellular trafficking of membrane-enclosed compartments, including secretory granules, endosomes, and lysosomes. Whole-exome sequencing in five families affected by mild to severe cutis laxa, dysmorphic facial features, and cardiopulmonary involvement identified biallelic missense mutations in *ATP6V1E1* and *ATP6V1A*, which encode the E1 and A subunits, respectively, of the $V_1$ domain of the heteromultimeric V-ATPase complex. Structural modeling indicated that all substitutions affect critical residues and inter- or intrasubunit interactions. Furthermore, complexome profiling, a method combining blue-native gel electrophoresis and liquid chromatography tandem mass spectrometry, showed that they disturb either the assembly or the stability of the V-ATPase complex. Protein glycosylation was variably affected. Abnormal vesicular trafficking was evidenced by delayed retrograde transport after brefeldin A treatment and abnormal swelling and fragmentation of the Golgi apparatus. In addition to showing reduced and fragmented elastic fibers, the histopathological hallmark of cutis laxa, transmission electron microscopy of the dermis also showed pronounced changes in the structure and organization of the collagen fibers. Our findings expand the clinical and molecular spectrum of metabolic cutis laxa syndromes and further link defective extracellular matrix assembly to faulty protein processing and cellular trafficking caused by genetic defects in the V-ATPase complex.

## Introduction

The V-type proton ($H^+$) ATPase (V-ATPase) is an ATP-dependent $H^+$ pump that establishes and maintains the acidic environment of intracellular organelles, including secretory granules, endosomes, and lysosomes, as well as extracellular compartments. This protein complex is composed of a catalytic cytosolic $V_1$ domain and a $H^+$-pumping, membrane-embedded $V_0$ domain, both of which comprise different subunits. The V-ATPase complex is essential to physiological processes such as membrane trafficking, protein degradation, pH homeostasis, and pH-dependent (e.g., Wnt and Notch) or -independent (e.g., mTORC1 and APMK) regulation of intracellular signaling, but it also mediates pathological processes including virus and toxin entry, drug resistance, and cancer cell survival, migration, and invasion.[1,2]

Gene mutations affecting V-ATPase have been identified in several autosomal-recessive (AR) Mendelian disorders.[3] In the $V_1$ domain, mutations affecting the B1 (*ATP6V1B1* [MIM: 192132]) and B2 (*ATP6V1B2* [MIM: 606939]) subunits cause AR distal renal tubular acidosis with early-onset

[1]Center for Medical Genetics, Ghent University and Ghent University Hospital, Ghent 9000, Belgium; [2]Department of Pediatrics, Radboud University Medical Center, Nijmegen 6500 HB, the Netherlands; [3]Department of Human Genetics, Radboud University Medical Center, Nijmegen 6500 HB, the Netherlands; [4]Radboud Center for Mitochondrial Medicine, Department of Pediatrics, Radboud University Medical Center, Nijmegen 6500 HB, the Netherlands; [5]Translational Metabolic Laboratory, Department of Laboratory Medicine, Radboud University Medical Center, Nijmegen 6500 HB, the Netherlands; [6]Childrens' Hospital, Klinikum am Steinenberg, Reutlingen 72764, Germany; [7]Kariminejad-Najmabadi Pathology & Genetics Center, Tehran 14656, Iran; [8]Department of Neurology, Radboud University Medical Center, Nijmegen 6500 HB, the Netherlands; [9]Department of Biomedical Molecular Biology, Ghent University, Ghent 9000, Belgium; [10]Inflammation Research Center, VIB, Ghent 9000, Belgium; [11]Hayward Genetics Center, Tulane University Medical School, New Orleans, LA 70112, USA; [12]Shahrood Genetic Counseling Center, Semnan 36156, Iran; [13]Department of Neuropediatrics, Children's Hospital Klinikum Oldenburg, Oldenburg 26133, Germany; [14]Department of Paediatrics & Adolescent Medicine, Li Ka Shing Faculty of Medicine, University of Hong Kong, Hong Kong, China; [15]Institute of Pathology, Universitätsklinikum Heidelberg, Heidelberg 69120, Germany; [16]Institute of Medical Genetics and Human Genetics, Charité – Universitaetsmedizin Berlin, Berlin 13353, Germany; [17]Max Planck Institute for Molecular Genetics, Berlin 14195, Germany; [18]Institute of Human Genetics, Helmholtz Zentrum München, Neuherberg 85764, Germany; [19]Pediatric Genetics Unit, Department of Pediatrics, Acibadem University School of Medicine, Istanbul 34752, Turkey; [20]Pediatric Genetics Unit, Department of Pediatrics, Ihsan Doğramacı Children's Hospital, Hacettepe School of Medicine, Ankara 06100, Turkey; [21]Center for Child and Adolescent Medicine, Klinik Kinderheilkunde I, Universitätsklinikum Heidelberg, Heidelberg 69120, Germany; [22]Institute of Human Genetics, Technische Universität München, Munich 81675, Germany; [23]Institute of Medical Genetics and Applied Genomics, University of Tübingen, Tübingen 72076, Germany; [24]Department of Pediatrics, University Hospital Leuven, Leuven 3000, Belgium
[25]These authors contributed equally to this work
[26]These authors contributed equally to this work
[27]These authors contributed equally to this work
*Correspondence: bert.callewaert@ugent.be (B.C.), ron.wevers@radboudumc.nl (R.A.W.)
http://dx.doi.org/10.1016/j.ajhg.2016.12.010.

hearing loss (MIM: 267300) and Zimmermann-Laband syndrome (MIM: 616455), respectively.[4,5] In the $V_0$ domain, mutations affecting the a4 subunit (*ATP6V0A4* [MIM: 605239]) cause AR distal renal tubular acidosis with late-onset hearing loss (MIM: 602722), whereas mutations in *TCIRG1* (MIM: 604592), encoding the osteoclast specific long isoform of the a3 subunit, cause AR osteopetrosis (MIM: 259700).[6,7] Finally, mutations in *ATP6V0A2* (MIM: 611716), encoding the a2 subunit of the $V_0$ domain, cause AR cutis laxa type 2A (ARCL2A [MIM: 219200]).[8] ARCL2A is a congenital disorder of glycosylation (CDG) characterized by a typical facial gestalt, skin abnormalities ranging from mild wrinkling to severe cutis laxa, and variable neurological and skeletal involvement. Genetic depletion of *ATP6V0A2* disrupts normal vesicular trafficking and results in abnormal glycosylation of serum proteins, intracellular accumulation of tropoelastin, reduced deposition of mature elastin in the extracellular matrix (ECM), accumulation of abnormal lysosomes and multivesicular bodies, and increased autophagy.[8,9] Cutis laxa syndromes are a heterogeneous group of acquired or inherited disorders with redundant or wrinkly skin and elastic-fiber fragmentation as their clinical and histopathological hallmarks. Heritable cutis laxa syndromes are caused not only by defects in ECM molecules (e.g., elastin) but also by defects in diverse metabolic pathways, such as intracellular trafficking, proline synthesis, and mitochondrial function.[10,11] Nevertheless, how these metabolic defects interfere with ECM assembly remains elusive.

Here, we report biallelic mutations in *ATP6V1E1* (MIM: 108746) and *ATP6V1A* (MIM: 607027), respectively encoding the E1 and A subunits of the $V_1$ domain of V-ATPase, as a cause of distinct metabolic and multisystemic cutis laxa entities. We show that these mutations affect V-ATPase structure and assembly, protein glycosylation, Golgi trafficking, and lysosomal function and lead to defects in ECM homeostasis and architecture.

## Subjects and Methods

### Clinical Assessment

All individuals were referred to one of the collaborating academic expert centers for diagnostic workup of cutis laxa. Blood samples were collected from seven affected individuals from five families and their unaffected parents (Figure 1). Skin biopsies were obtained from PI:1, PIII:1, PIV:1, and one individual with compound-heterozygous c.1214C>T (p.Pro405Leu) and c.1529G>T (p.Arg510Ile) *ATP6V0A2* mutations (PV0A2; reported as patient 1 in Hucthagowder et al.[9]). PCR-based next-generation sequencing of known cutis-laxa-related genes did not identify causal mutations in the probands of families I and III. The study was conducted in accordance with the Declaration of Helsinki, and informed consent was obtained from all affected individuals and/or parents.

### Whole-Exome Sequencing

Whole-exome sequencing (WES) was performed on genomic DNA extracted from blood leukocytes of the probands of each family on four different platforms. Details on exome capture, sequencing, and variant filtering in all families are available on request. Variants were annotated with PolyPhen-2, SIFT, MutationTaster, Align-GVGD, MAPP (Multivariate Analysis of Protein Polymorphism), and variant allele frequencies from the Exome Aggregation Consortium (ExAC) Browser and our in-house exome cohorts.[12–18] Sequence validation and segregation analysis of the candidate variants were performed with Sanger sequencing (reference sequences GenBank: NM_001696.3 [*ATP6V1E1*] and NM_001690.3 [*ATP6V1A*]). Variant nomenclature adheres to the Human Genome Variation Society (HGVS) guidelines, and all variants were checked with Mutalyzer software (version 2.0.18).[19]

### Expression Analysis

For quantitative reverse-transcription PCR (qRT-PCR), total RNA was extracted in triplicate from cultured fibroblasts with the RNeasy Kit (QIAGEN), and cDNA was synthesized with the iScript cDNA Synthesis Kit (Bio-Rad Laboratories). For each cDNA sample, assays were prepared with the addition of RealTime ready DNA Probes Master mix and ResoLight Dye (Roche) and were subsequently run in duplicate on a Roche LightCycler 480 System. Data were analyzed with qbase+ (version 3.0, Biogazelle) and *HPRT1*, *RPL13A*, and *YWHAZ* as reference genes.

### Immunoblotting

For immunoblotting of the E1 and A subunits, total protein was extracted with Laemmli Sample Buffer (Bio-Rad Laboratories) and subjected to SDS-PAGE. Proteins were transferred to a nitrocellulose membrane with the iBlot 2 Dry Blotting System (Thermo Fisher Scientific). Membranes were blocked in 2% ECL Blocking Agent (GE Healthcare), incubated with Abcam primary antibodies against ATP6V1E1 (1:200; ab176789), ATP6V1A (1:2,000; ab199326), or β-tubulin (1:1,000; ab6046), and subsequently incubated with horseradish-peroxidase-conjugated secondary antibody (1:1,500; 7074S, Cell Signaling Technologies). Membranes were scanned with a ChemiDoc-It 500 Imaging System (UVP), and signal intensity was compared to the amount of β-tubulin.

### Structural Modeling

Homology models of the E1 and A subunits of the human V-ATPase were generated with I-Tasser software (Iterative Threading ASSEmbly Refinement) with the respective subunits of the *Saccharomyces cerevisiae* V-ATPase (PDB: 3J9T) as a template.[20–23] The homology models were subsequently inserted in and aligned to the available three-dimensional structure of the *S. cerevisiae* V-ATPase with the MatchMaker function of the UCSF Chimera software package (version 1.10.2, build 40686).[24] The Dunbrack rotamers function was used to substitute specific residues within the protein structure to model the effect of the specific protein variants.[25] The FindHBond function was used to identify potential hydrogen bonds.

### Complexome Profiling

For preparation of a cellular fraction enriched with V-ATPase subunits, frozen fibroblast pellets were resuspended in ice-cold 125 mM sucrose and 10 mM Tris-HCl (pH 7.4) and incubated for 5 min on ice. The cells were homogenized with ten strokes at 1,800 rpm with a glass and Teflon homogenizer at 0°C. The homogenate was mixed with 1.5 M sucrose at a ratio of 8:1 and subsequently centrifuged at 1,000 × *g* at 4°C for 10 min for the removal of nuclei, cell debris, and intact cells. The supernatant was again centrifuged at 6,000 × *g* at 2°C for 10 min, after which the supernatant was pelleted by ultra-speed centrifugation at


**Figure 1. Clinical Characteristics and Pedigrees**
Clinical pictures of PI:1 (at birth, A–E), PII:1 (at age 10 years, F–H), PII:2 (at age 9 years, I and J), PIII:1 (at birth, K and L; at age 15 years, M), and PIV:1 (at birth, N–Q) and pedigrees of all affected families. Clinical pictures of PV:1 were not available.

240,000 × *g* at 4°C for 60 min. The obtained pellet, enriched with V-ATPase subunits, was resuspended in 250 mM sucrose and 10 mM Tris-HCl (pH 7.4). Protein concentration was determined by the Lowry method. Complexome profiling with liquid chromatography tandem mass spectrometry after blue-native PAGE (4%–16%) was performed as described previously.[26,27]

## Glycosylation Screening

Isoelectric focusing of plasma transferrin and apolipoprotein CIII (ApoCIII) was performed for the screening of defects in protein N-glycosylation and mucin type O-glycosylation, respectively.[28–30] In addition, quadrupole-time-of-flight mass spectrometry of intact transferrin was performed as described previously.[30]

## Immunocytochemistry

For Golgi-trafficking studies, fibroblasts were seeded in eight-well Nunc Lab-Tek chamber slides (Thermo Fisher Scientific) and grown under standard conditions. At confluency, samples were incubated with 5 μg/mL brefeldin A (B5936, Sigma-Aldrich) for 6 min at 37°C and fixed with ice-chilled absolute methanol. Fixed samples were blocked with 10% (w/v) bovine serum albumin (BSA; Sigma-Aldrich), incubated with primary antibody against GOLPH4 (1:400; ab28049, Abcam), and subsequently incubated with an Alexa-Fluor-594-conjugated secondary antibody (1:1,500; A-21207, Life Technologies). Nuclei were counterstained with DAPI (Life Technologies). Images were analyzed with a Zeiss Axio Observer.Z1 microscope. For each cell line, 150 brefeldin-A-treated cells were scored independently by three observers on the presence or absence of Golgi remnants.

For immunocytochemical analysis of intercellular adhesion molecule 1 (ICAM-1), fibroblasts were seeded on glass coverslips and cultured for 5 days. On day 6, they were fixed with 4% formaldehyde (Sigma-Aldrich) and permeabilized with 0.1% (w/v) saponin and 0.1% (w/v) BSA. Samples were blocked in 5% (w/v) normal donkey serum (Jackson ImmunoResearch Laboratories),

incubated with a primary antibody against ICAM-1 (1:750; MA5-13021, Thermo Fisher Scientific), and subsequently incubated with a biotinylated donkey anti-mouse secondary antibody (1:800; 715-065-151, Jackson ImmunoResearch Laboratories) and streptavidin-conjugated Cy3 (1 μg/mL; 016-160-084, Jackson ImmunoResearch Laboratories). The samples were mounted with VECTASHIELD Mounting Medium containing DAPI (Vector Laboratories). Images were obtained with an Olympus BX51 System Microscope. Particle analysis and manual counting were performed with Fiji and the Cell Counter plugin (version 2.0.0-rc-49/1.51a).[31–33]

### Transmission Electron Microscopy

Samples were fixed in 4% paraformaldehyde and 2.5% glutaraldehyde in 0.1 M sodium cacodylate buffer (pH 7.2). After being washed in buffer solution, samples were postfixed in 1% $OsO_4$ with $K_3Fe(CN)_6$ in 0.1 M sodium cacodylate buffer (pH 7.2) and subsequently dehydrated through a graded ethanol series, including a bulk staining with 2% uranyl acetate at the 50% ethanol step followed by embedding in Spurr's resin. Ultrathin sections of a gold interference color were cut with an EM UC6 ultramicrotome (Leica Microsystems) and then consecutively stained with uranyl acetate and lead stain in a Leica EM AC20. Sections collected on formvar-coated copper slot grids were viewed with a JEOL JEM 1400plus transmission electron microscope operating at 60 kV.

## Results

### Clinical Phenotype

Table 1, Figure 1, and Figure S1 summarize and illustrate the salient clinical findings in all seven affected individuals. Detailed case reports are available in the Supplemental Note.

At birth, anthropometric parameters were mostly within normal range. Perinatal complications were reported in several families. PI:1 and PIV:1 died after several months of intensive care and treatment. In family I, a second pregnancy (PI:2) was terminated at 21 weeks of gestation because of cardiac abnormalities and increased nuchal thickness. The siblings from family II were admitted shortly after birth with respiratory distress secondary to bilateral pneumothoraxes, and in PIV:1, the neonatal course had been complicated by seizures, pneumonia, sepsis, and a half-hour-long resuscitation after a dislocated endotracheal tube.

All affected individuals presented with generalized skin wrinkling and sparse subcutaneous fat. In addition, PIII:1, PIV:1, and PV:1 had large skin folds and abnormal fat distribution, especially on the buttocks. With the exception of PIII:1, who had milder facial features, all affected individuals had a similar progeroid facial gestalt with a "mask-like" triangular face, a short forehead, hypertelorism, entropion, low-set ears with misfolded helices, a beaked nose with a broad nasal base and narrow nostrils, and a short and pointed chin.

At birth, several affected individuals had congenital heart defects including septal defects (PII:1, PIV:1, and PV:1), cardiac valve defects (PII:1), and right hypoplastic heart syndrome (PI:2). Other cardiovascular complications included dilatation of the ascending aorta (PI:1 and PIV:1), hypertrophic cardiomyopathy (PI:1 and PIII:1), dilatation of the right ventricle and reduced diastolic compliance (PII:1), and cardiac failure (PIV:1).

Three families had a history of neurologic complications. PIII:1 had a severe speech delay, and he suffered a generalized tonic-clonic seizure at the age of 14 years. MRI showed enlarged ventricles with white-matter involvement and periventricular parieto-occipital gliosis. PIV:1 developed epileptic seizures shortly after birth, which evolved to generalized and complex partial seizures at the age of 2 months. MRI showed diffuse thickening of the cerebral cortex, suggestive of polymicrogyria, and a thin corpus callosum. Finally, in PV:1, MRI showed an anatomical variant of the cavum septum pellucidum.

Most affected individuals suffered from severe and often disabling hypotonia. Additional but less frequent features included hip dysplasia (PI:1, PII:1, and PIV:1), multiple congenital contractures (PI:1 and PIV:1), kyphoscoliosis (PII:1 and PII:2), marfanoid habitus (PII:1, PII:2, and PIII:1), inguinal herniation (PII:2 and PIV:1), and cryptorchidy (PII:2 and PIV:1).

### Biallelic Mutations in *ATP6V1E1* and *ATP6V1A* Cause Cutis Laxa

WES revealed biallelic missense variants in *ATP6V1E1* (GenBank: NM_001696.3) and *ATP6V1A* (GenBank: NM_001690.3), encoding the E1 and A subunits, respectively, of the V-ATPase complex (Figures 2A and 2D and Table S2). *ATP6V1E1* and *ATP6V1A* were considered strong candidate genes because mutations in *ATP6V0A2*, encoding another subunit of the same complex, are known to cause ARCL2A.[8] PI:1 (family I) and PII:1 (family II) harbored homozygous variants in *ATP6V1E1*: a c.383T>C (p.Leu128Pro) and c.634C>T (p.Arg212Trp), respectively. The other three families had homozygous *ATP6V1A* variants. In PIII:1 (family III), WES identified a c.1012C>T (p.Arg338Cys) variant, whereas PIV:1 (family IV) and PV:1 (family V) had missense variant c.215G>A (p.Gly72Asp). All variants segregated as expected for pathogenic AR mutations, were designated as disease causing by the majority of in silico predictions algorithms, were confirmed to affect highly conserved amino acids, and had not been reported in the ExAC Browser or our in-house exome cohorts (Figure 2D and Table S2).[18] The p.Arg212Trp substitution in the E1 subunit had been reported as a potential pathogenic mutation in a single family affected by cutis laxa.[34] Although both genes are ubiquitously expressed, RT-PCR detected higher expression in skin and cultured fibroblasts, which is in agreement with the severe cutis laxa phenotype (Figure S2). Notably, expression of *ATP6V1E2*, which encodes the second isoform of the E subunit, was relatively low and restricted to the testes.

**Table 1. Overview of Genotypes, Clinical Characteristics, and Experimental Findings**

| | PI:1 | PI:2 | PII:1 | PII:2 | PIII:1 | PIV:1 | PV:1 | ARCL2A |
|---|---|---|---|---|---|---|---|---|
| Sex | female | female | female | male | male | male | male | NA |
| Ethnicity | Iranian | Iranian | Kuwaiti | Kuwaiti | German | Pakistani | Turkish | NA |
| Age at last evaluation | 5 months | fetus | 10 years | 9 years | 15 years | 3 months | ? | NA |
| **Genotype** | | | | | | | | |
| Gene | *ATP6V1E1* | *ATP6V1E1* | *ATP6V1E1* | *ATP6V1E1* | *ATP6V1A* | *ATP6V1A* | *ATP6V1A* | *ATP6V0A2* |
| cDNA change | c.383T>C | c.383T>C | c.634C>T | c.634C>T | c.1012C>T | c.215G>A | c.215G>A | NA |
| Zygosity | homozygous | homozygous | homozygous | homozygous | homozygous | homozygous | homozygous | biallelic |
| Protein change | p.Leu128Pro | p.Leu128Pro | p.Arg212Trp | p.Arg212Trp | p.Arg338Cys | p.Gly72Asp | p.Gly72Asp | NA |
| **Clinical Phenotype** | | | | | | | | |
| Generalized cutis laxa | + | − | + | + | + | + | + | +/− |
| Large skin folds | − | − | − | − | + | +/− | + | − |
| Improving cutis laxa with age | ND | − | ND | ND | + | ND | ND | − |
| Facial dysmorphology[a] | + | +/− | + | + | +/− | + | + | + |
| Entropion | + | ND | + | + | − | − | + | − |
| Hip dysplasia | + | ND | + | − | − | + | − | + |
| Contractures | + | − | − | − | − | + | − | − |
| Kyphoscoliosis | − | − | + | + | − | − | − | + |
| Marfanoid habitus | − | − | + | + | + | − | − | − |
| Hypotonia | + | ND | + | + | + | + | + | + |
| Cardiac abnormalities | + | + | + | − | + | + | + | − |
| Aortic dilation | + | − | − | − | − | + | − | − |
| Pneumothorax | ND | − | + | + | ND | ND | ND | − |
| Seizures | ND | ND | ND | ND | + | + | ND | + |
| MRI abnormalities | ND | ND | − | ND | + | + | +/− | + |
| Urogenital abnormalities[b] | − | − | − | + | ND | + | ND | − |
| **Cellular Phenotype** | | | | | | | | |
| TIEF abnormalities | ND | ND | type II | type II | +/− | +/− | ND | type II |
| MS abnormalities | ND | ND | + | + | + | + | ND | + |
| ICAM-1 reduction | + | ND | ND | ND | + | ND | ND | NR |
| Golgi-trafficking defects | + | ND | ND | ND | + | ND | ND | + |
| Giant autolysosomes | + | ND | ND | ND | − | ND | ND | +/− |
| ECM defects | + | ND | ND | ND | + | + | ND | + |

Abbreviations are as follows: +, present; −, absent; +/−, mildly or variably present; ?, unknown; NR, not reported; NA, not applicable; ND, not determined; TIEF, transferrin isoelectric focusing; MS, mass spectrometry; and ECM, extracellular matrix.
[a]Facial dysmorphology is characterized by a "mask-like" triangular face, a short forehead, hypertelorism, entropion, low-set ears with misfolded helices, a beaked nose with a broad nasal base and narrow nostrils, and a short and pointed chin.
[b]Inguinal herniation and cryptorchidy.

### *ATP6V1E1* and *ATP6V1A* Mutations Affect Critical Residues in the V-ATPase Complex

We mapped the identified mutations on homology models of the E1 and A subunits (Figure 2D). In the E1 subunit, the Leu-to-Pro substitution at position 128 disrupts a hydrophobic interaction at the interface between the C-terminal globular domain of the E1 subunit and the opposing B subunit. The Arg-to-Trp substitution at position 212 is predicted to break a salt-bridge interaction with Asp88, which is located in the N-terminal region of the same subunit. In the A subunit, the substitution of an Arg residue with a Cys residue at position 338 seems to break salt-bridge interactions with Glu335 and Asp339, which are located

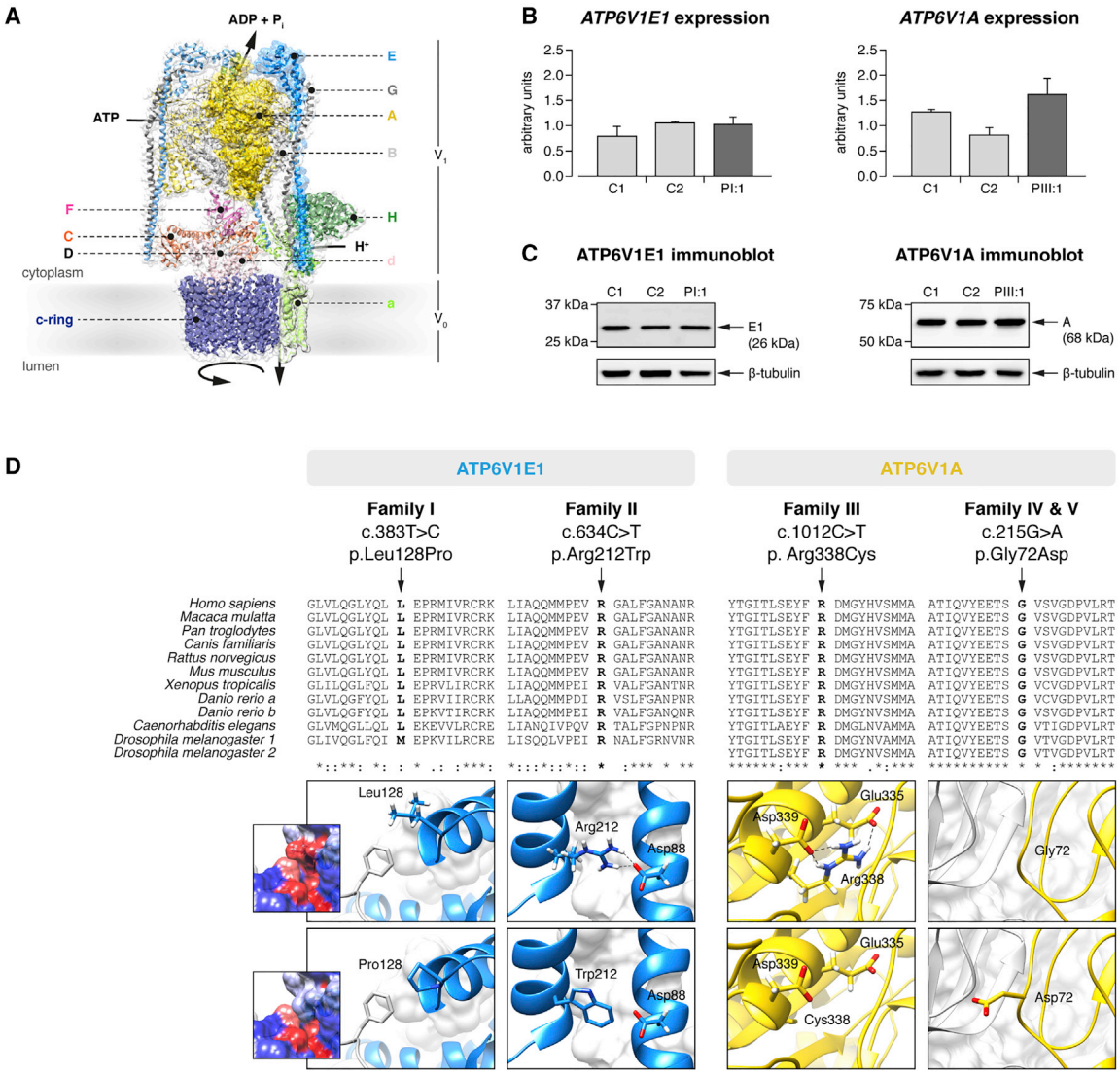


**Figure 2.** ***ATP6V1E1* and *ATP6V1A* Mutations**

(A) Alignment of I-Tasser homology models for the human E1 (blue surface shading) and A (yellow surface shading) subunits with a three-dimensional model of the *Saccharomyces cerevisiae* V-ATPase (PDB: 3J9T).[23]

(B) qRT-PCR analysis of *ATP6V1E1* and *ATP6V1A* in cultured fibroblasts from PI:1, PIII:1, and two age- and sex-matched control individuals showed no difference in expression. Data are expressed as the mean, and error bars represent the 95% confidence interval.

(C) Immunoblotting against the E1 and A subunits in PI:1, PIII:1, and two age- and sex-matched control individuals showed no difference in protein level in cultured fibroblasts.

(D) Clustal Omega protein sequence alignment and structural modeling. The protein sequence of the E1 and A subunits is highly conserved across vertebrates and invertebrates, and all affected amino acid residues are evolutionary highly conserved. Asterisks indicate a single, fully conserved residue, colons indicate strong similar properties (>0.5 in the Gonnet PAM 250 matrix), and periods indicate weak similar properties (≤0.5 in the Gonnet PAM 250 matrix). Structural modeling indicated that all identified mutations affect critical residues within the E1 or A subunit and disrupt inter- or intrasubunit interactions within the V-ATPase complex.

within the same α-helical region of the nucleotide-binding domain of the subunit. The last substitution is predicted to change a nonpolar Gly residue in the N-terminal domain (position 72) to a basic Asp residue at the interface between the A and B subunits. Therefore, all substitutions are predicted to affect critical residues and destabilize inter- or intrasubunit interactions in the V-ATPase complex.

### *ATP6V1E1* and *ATP6V1A* Mutations Alter V-ATPase Stability

*ATP6V1E1* and *ATP6V1A* expression and protein levels of the E1 and A subunits were unaffected in PI:1 and PIII:1 (Figures 2B and 2C). We therefore studied the abundance and stability of the V-ATPase by complexome profiling (Figure 3). In all samples, we identified all eight subunits of the $V_1$ domain, the three subunits of the $V_0$ domain

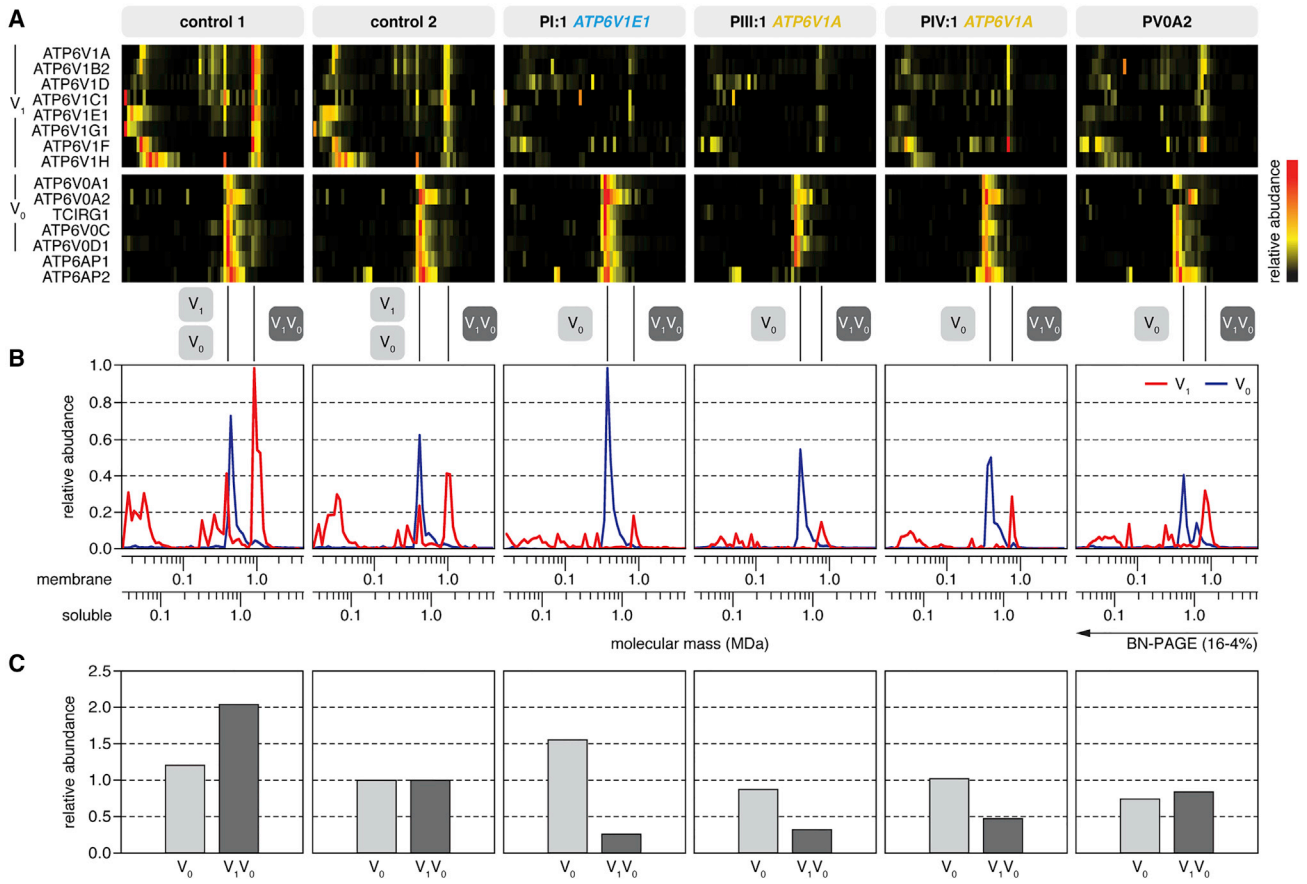


**Figure 3. Complexome Profiling**

(A) Heatmap representations of the migration profiles of the identified $V_1$ and $V_0$ subunits and two V-ATPase assembly factors (ATP6AP1 and ATP6AP2) were created by hierarchical clustering and, for proteins that were not grouped together by the clustering algorithm, by correlation profiling. In control fibroblast cultures, the fully assembled V-ATPase and the separate $V_1$ and $V_0$ domains migrated with apparent molecular masses of 1,000, 600, and 450 kDa, respectively. The majority of $V_1$ subunits were integrated in the complete V-ATPase complex, whereas the vast majority of $V_0$ subunits were integrated in the $V_0$ subassembly. In fibroblast cultures from individuals with *ATP6V1E1* or *ATP6V1A* mutations, the abundance of $V_1$ subunits was markedly lower than in control individuals.

(B) Migration profiles of the $V_1$ (red) and $V_0$ (blue) domains show the average value of the abundance of the detected subunits of the respective fraction plotted against the molecular mass.

(C) The amount of fully assembled V-ATPase complex was markedly reduced in fibroblast cultures from all individuals with *ATP6V1E1* or *ATP6V1A* mutations, but the amount of $V_0$ domain was unchanged. In PV0A2, an individual with compound-heterozygous *ATP6V0A2* mutations, the amount of fully assembled V-ATPase complex was only moderately reduced. To calculate the values, we summarized the abundances of all detected subunits in the respective fraction and normalized them to control 2.

(including three isoforms of subunit a), and two accessory subunits (Figure 3A and Table S1). In two control fibroblast cultures, we identified the fully assembled V-ATPase and the separate $V_1$ and $V_0$ domains migrating with apparent molecular masses of 1,000, 600, and 450 kDa, respectively (Figure 3B). In addition, we detected two subassemblies of the $V_1$ domain: a larger one lacking subunits F and H and a smaller one lacking the peripheral stalk subunits E and G. About two-thirds of the $V_1$ domain was integrated in the complete V-ATPase complex, whereas the vast majority of $V_0$ domains appeared as a separate entity. Moreover, we observed a larger variant of the $V_0$ domain, which might be a dimer of this subdomain, containing only isoform 2 of subunit a. In PI:1, PIII:1, and PIV:1, the overall abundance of the $V_1$ subunits and the fully assembled V-ATPase complex was markedly reduced, but the amount of $V_0$ domain either increased or hardly changed (Figure 3B). In the individual with compound-heterozygous *ATP6V0A2* mutations (PV0A2), the abundance of the fully assembled V-ATPase complex was moderately reduced, but the affected a2 isoform was entirely absent from the $V_0$ domain monomer and appeared associated with the larger variant of the $V_0$ domain.

### *ATP6V1E1* and *ATP6V1A* Mutations Result in Glycosylation Abnormalities

Isoelectric focusing of transferrin and ApoCIII showed variable glycosylation abnormalities (Tables 1 and S3). The two family II siblings with a defect in the E1 subunit (PII:1 and PII:2) had a clearly abnormal transferrin isoelectric focusing pattern with decreased tetrasialotransferrin

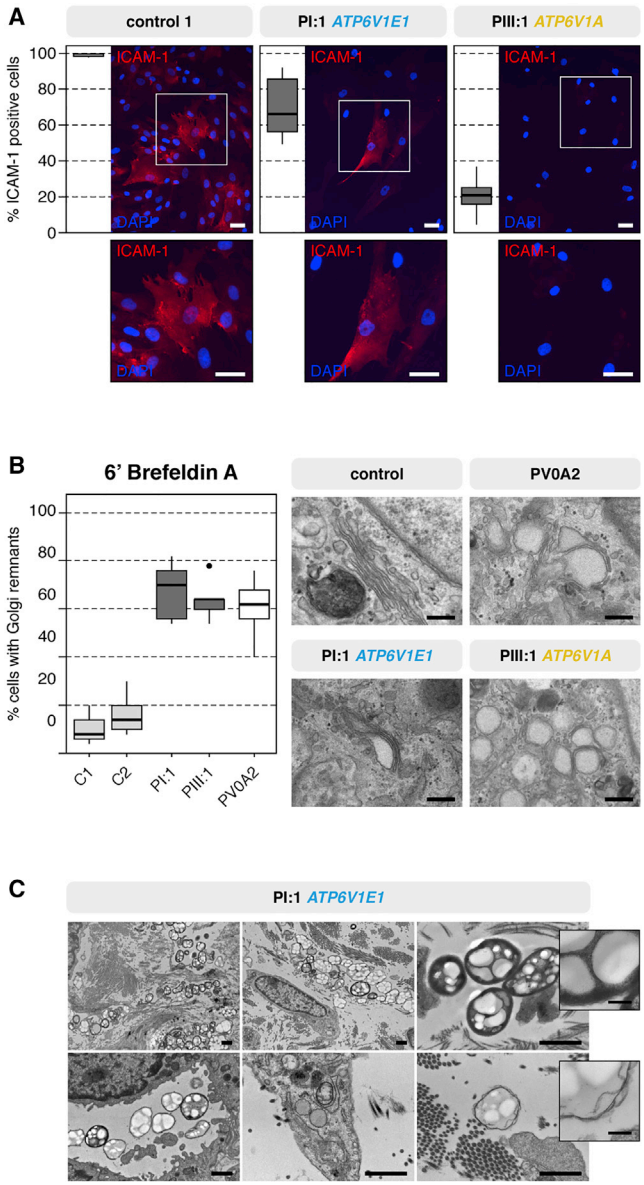


**Figure 4. Glycosylation and Vesicular Trafficking Studies**
(A) Immunocytochemistry of the highly glycosylated ICAM-1 showed a severe reduction in the percentage of ICAM-1-positive fibroblasts. Scale bars represent 25 μm.
(B) Retrograde translocation of Golgi membranes to the endoplasmic reticulum was severely delayed in brefeldin-A-treated fibroblasts from PI:1 and PIII:1. Similar to PV0A2 (with ARCL2A), PI:1 and PIII:1 showed a 2- to 3-fold higher percentage of cells retaining Golgi remnants than control individuals. Additionally, TEM showed dilated and fragmented Golgi cisternae in PI:1, PIII:1, and PV0A2. Scale bars represent 250 nm.
(C) TEM imaging of the dermis of PI:1 showed the presence of large, heterogeneous vacuolar structures within or near fibroblasts and in the endothelial lumen. Scale bars represent 1 μm or 200 nm (inset).

and increased di- and trisialiotransferrin (Table S3). This pattern is indicative of a type II CDG. ApoCIII isoelectric focusing for evaluation of mucin-type O-glycosylation was normal in PII:1 and showed a minimal increase in the ApoCIII-0 fraction in PII:2 (Table S3). Similar but milder N-glycosylation abnormalities were observed in the individuals with a defect in the A subunit (Tables 1 and S3). For PIII:1, samples were taken at three different ages. All samples showed a slightly increased trisialotransferrin fraction but normal tetrasialotransferrin levels. ApoCIII isofocusing was normal at the age of 7 years, but fully glycosylated ApoCIII was slightly decreased at the age of 13 years. In PIV:1, a marginal increase in the trisialotransferrin was observed, and ApoCIII analysis was normal.

In all affected individuals, mass spectrometry of intact transferrin revealed a consistent increase in the abundance of the transferrin glycoform, corresponding to the loss of one sialic acid (mass 79,264 amu; Figure S3). In addition, a minor lack of galactose was observed in family II (PII:1 and PII:2), which is in agreement with known disorders of Golgi trafficking (Figure S3).

In CDGs, there is a markedly reduced amount of the cell-surface glycoprotein ICAM-1.[35] There was a significant decrease in the number of ICAM-1-positive cells on immunofluorescence microscopy in both PI:1 and PIII:1 (Figure 4A).

### *ATP6V1E1* and *ATP6V1A* Mutations Disrupt Vesicular Trafficking

Fluorescence microscopy of the Golgi marker GOLPH4 did not show abnormal Golgi morphology. Transmission electron microscopy (TEM) of fibroblast cultures, however, showed abnormal swelling and a fragmented appearance of the Golgi apparatus in PI:1 and PIII:1 (Figure 4B). In line with previous studies on ARCL2A fibroblasts, we observed delayed retrograde vesicular transport between the Golgi and endoplasmic reticulum in cultured fibroblasts from PI:1 and PIII:1: after brefeldin A treatment, the number of cells retaining Golgi remnants was two to three times higher than in control samples (Figure 4B).[8,36]

Additionally, in PI:1, but not in PIII:1 or PIV:1, we observed large heterogeneous vacuolar structures within or in close proximity to fibroblasts or in the lumen of blood vessels on TEM of skin biopsies (Figure 4C). These resembled large autolysosomes or lysosomal storage bodies, which are seen in lysosomal-storage disease.

### *ATP6V1E1* and *ATP6V1A* Mutations Variably Affect ECM Assembly

Both pharmacological V-ATPase inhibition with bafilomycin A1 and genetic depletion of the a2 subunit reduce tropoelastin secretion, but their structural impact on ECM architecture has never been studied thoroughly.[5,30] The elastic fibers appeared normal in structure and amount in PIII:1 but were irregular, fragmented, and reduced in PIV:1 and—with the exception of some very small fragments—absent in PI:1 (Figure 5). In all samples, collagen fibrils were loosely packed and had more variable diameters than the tightly assembled and regularly organized collagen fibrils in control samples (Figure 5). Overall,

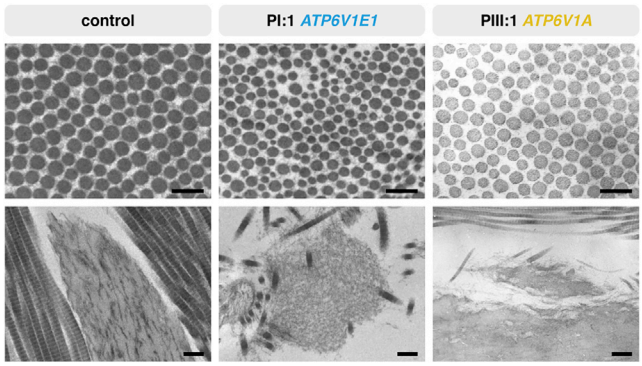


**Figure 5. Ultrastructural Studies of the ECM**
TEM of the dermis of PI:1 and PIII:1 showed collagen abnormalities with increased interfibrillar space and more variable fibril diameters than did a control sample (top row; scale bars represent 250 nm). Elastic fibers appeared normal in PIII:1 but were very irregular, fragmented, and almost absent in PI:1 (bottom row; scale bars represent 500 nm).

the ECM also appeared much less compact in PI:1 and PIV:1.

## Discussion

We have described homozygous mutations in *ATP6V1E1* and *ATP6V1A*, encoding the E1 and A subunits, respectively, of the V-ATPase complex, in four individuals (two families) and three individuals (three families) with cutis laxa and multisystemic involvement. In infancy, both entities showed considerable clinical overlap with generalized cutis laxa, similar facial features, hypotonia, joint contractures, and congenital hip dysplasia. However, *ATP6V1E1* mutations cause generalized skin wrinkling, whereas the cutis laxa pattern in affected individuals with *ATP6V1A* mutations is characterized more by large skin folds and abnormal fat distribution and seems to improve over time. *ATP6V1A* mutations also affect the central nervous system. Finally, both entities infer a risk of potentially life-threatening cardiopulmonary complications, such as pneumothorax, aortic root dilatation, cardiomyopathy, and congenital heart defects. The latter features also differentiate *ATP6V1E1*- and *ATP6V1A*-related cutis laxa from the more classic and prevalent ARCL2A, caused by mutations in *ATP6V0A2*. Individuals with ARCL2A rarely show cardiopulmonary involvement. The cardiopulmonary features in *ATP6V1E1*- and *ATP6V1A*-related cutis laxa are, however, also distinct from those reported in ARCL-type-1-affected individuals, who present with emphysema, arterial tortuosity, aneurysms, and stenosis, and we therefore propose to include these cutis laxa syndromes in ARCL type 2.[37]

*ATP6V1E1*, *ATP6V1A*, and *ATP6V0A2* encode different subunits of the V-ATPase pump, whose complexity is exemplified in part by its structural organization in two functional domains each comprising several subunits with tissue-specific isoforms. We have shown that human *ATP6V1E1* and *ATP6V1A* are widely expressed, which parallels the pleiotropic manifestations reported here. Notably, the expression of mouse *Atp6v1e1* and its protein product was previously shown to be restricted to developing and mature acrosomes, but this corresponds to the testis-specific expression of human *ATP6V1E2* reported here.[38]

The identified homozygous mutations in *ATP6V1E1* and *ATP6V1A* affect highly conserved amino acids within the E1 and A subunits, respectively, seem to disrupt stabilizing interactions within or between different subunits of the nucleotide-binding domain (trimer of AB heterodimer) or peripheral stalks (EG heterodimers), and thereby probably reduce ATP-hydrolysis-coupled $H^+$ transport.[23] The peripheral stalks tether the nucleotide-binding $A_3B_3$ domain to the $V_0$ membrane domain to counteract the torque generated on the latter by the rotatory stalk units D and F during ATP hydrolysis. In addition, defects in the E1 and A subunits also interfere with the assembly and structure of the entire V-ATPase complex. Although expression of the genes encoding the affected subunits was normal, complexome profiling showed a markedly reduced abundance of the assembled $V_1$ domain and the complete membrane-bound $V_1V_0$ complex in cultured fibroblasts from individuals with *ATP6V1E1* or *ATP6V1A* mutations, whereas the abundance of the V-ATPase complex was only mildly affected in cells from an individual with ARCL2A (PV0A2). Interestingly, biallelic mutations affecting (putative) assembly factors of the V-ATPase complex have also been associated with disease and have been identified in X-linked myopathy with excessive autophagy (XMEA; *VMA21* [MIM: 300913]) and more recently in liver disease with (*ATP6AP1* [MIM: 300197]) or without (*TMEM199* [MIM: 616815] and *CCDC115* [MIM: 613734]) immune deficiency.[39–42] Our data also show that complexome profiling could contribute to the functional evaluation of gene mutations affecting V-ATPase by shedding light on their detailed molecular consequences and, as such, their pathogenicity.[26]

Similar to mutations in *ATP6V0A2*, mutations in *ATP6V1E1* and, to a lesser extent, *ATP6V1A* affect the glycosylation of proteins, suggesting that V-ATPase defects are in part CDGs.[43] We therefore propose including them in the current CDG classification as *ATP6V1E1*- and *ATP6V1A*-related CDG. Routine glycosylation screening by means of transferrin isoelectric focusing showed a pattern indicative of a CDG type II in individuals with *ATP6V1E1* mutations. N-glycosylation was, however, affected to a lesser extent in individuals with *ATP6V1A* mutations. Although glycosylation defects could therefore be missed by transferrin isoelectric-focusing techniques, abnormal transferrin glycosylation was evident on mass spectrometry analysis. Two observations could explain the variable N-glycosylation defects. First, the V-ATPase complex is structurally organized in two domains each composed of different subunits. These subunits have tissue-specific isoforms that enable different functions and

processes.[1–3] Our complexome profiling data illustrate that different mutations affect the assembly of the holocomplex to different extents.

Interestingly, pneumothorax, marfanoid habitus, aortic root dilatation, and ventricular dysfunction are all frequent manifestations of Marfan syndrome (MFS [MIM: 154700]), a disorder caused by heterozygous mutations in *FBN1* (MIM: 134797), encoding fibrillin-1. Fibrillin-1 is a highly glycosylated protein and co-assembles with several other glycoproteins and elastin to form elastic fibers. As such, disturbed glycosylation of proteins such as fibrillin-1 might explain the ultrastructural changes and clinical overlap with MFS. We observed variable ultrastructural abnormalities in the elastic and collagen fibers of dermal skin samples from the affected individuals. Although neither elastin nor collagen is heavily glycosylated, both depend on other glycosylated proteins for their secretion and assembly into the ECM.

Impaired retrograde Golgi trafficking was first reported in ARCL2A and has now been confirmed in these novel ARCL entities.[8,36] V-ATPases, however, acidify many other organelles, which makes it likely that disturbed pH regulation results in impaired enzymatic and sorting processes in many of these.[8] Notably, electron microscopy showed a significant amount of vacuolar structures, resembling autolysosomes, both intracellularly and in the vicinity of fibroblasts in infant PI:1. The presumed autolysosomes were not present in the other, older individuals, whose dermal phenotype had improved over time, and their presence might thus be a consequence of high protein synthesis and turnover in early life. These ultrastructural observations are supported by several studies. First, a recent study in *Drosophila melanogaster* showed that genetic V-ATPase defects interfere with lysosomal degradation and recycling and eventually lead to the formation of giant autolysosomes.[44] Second, lysosomal dysfunction is a driver in the pathogenesis of XMEA, which is caused by recessive mutations affecting the V-ATPase assembly factor VMA21.[41] Third, gingival hypertrophy is a prominent feature in *ATP6V1B2*-related Zimmerman-Laband syndrome and might relate to storage disease. Finally, the concomitant intracellular aggregation of tropoelastin and accumulation of abnormal lysosomes in ARCL2A might suggest secretion of tropoelastin via secretory lysosomes rather than secretory vesicles.[45] These findings implicate lysosomal dysfunction in the pathogenesis of these disorders and provide new insights in the cellular processes involved in proper assembly and homeostasis of the ECM. Further research is needed, however, to get more insight in the exact role of lysosomes in these disorders.

In conclusion, we have identified homozygous mutations in *ATP6V1E1* and *ATP6V1A*, respectively encoding the E1 and A subunits of the V-ATPase complex. Affected individuals presented with a recognizable and multisystemic cutis laxa phenotype overlapping ARCL2A. We have shown that these defects interfere with the assembly and functioning of the V-ATPase complex, protein glycosylation, intracellular trafficking, and lysosomal function.

## Supplemental Data

Supplemental Data include a Supplemental Note, two figures, and three tables and can be found with this article online at http://dx.doi.org/10.1016/j.ajhg.2016.12.010.

## Acknowledgments

The authors wish to thank Martin Lammens (Department of Pathology, Antwerp University Hospital and University of Antwerp) for his advice on the ultrastructural studies, Zsolt Urban (Department of Human Genetics, Graduate School of Public Health, University of Pittsburgh) for checking the DNA of a number of individuals with cutis laxa, and Angel Ashikov (Department of Neurology, Radboud University Medical Center) for his advice on subcellular fractionation. B.C. and F.M. are senior clinical investigators and D.S. is a postdoctoral researcher of the Fund for Scientific Research – Flanders. This study was financially supported by Ghent University (Methusalem grant 08/01M01108 to A.D.P.), the Dutch Metakids foundation (M.M.), the Netherlands Organisation for Scientific Research (NWO project 017.008.052 to M.M.), ZonMw Medium Investment Grant 40-00506-98-9001 (D.J.L.), Vidi grant 91713359 (D.J.L.), the Dutch Stofwisselkracht foundation (T.G.), the German Bundesministerium für Bildung und Forschung (BMBF, Juniorverbund in der Systemmedizin "mitOmics," FKZ 01ZX1405C to T.B.H.), the S.K. Yee Medical Research Fund, the Society for the Relief of Disabled Children Research Fund in Hong Kong, and the EURO-CDG-2 E-Rare grant by the European Commission. The authors would like to thank the Exome Aggregation Consortium and the groups that provided exome variant data for comparison. A full list of contributing groups can be found at http://exac.broadinstitute.org/about.

Received: September 21, 2016
Accepted: December 8, 2016
Published: January 5, 2017

## Web Resources

Align GVGD, http://agvgd.hci.utah.edu
GenBank, https://www.ncbi.nlm.nih.gov/genbank/
HGVS Nomenclature, http://www.hgvs.org/mutnomen/
OMIM, http://www.omim.org
MAPP, http://www.ngrl.org.uk/Manchester/page/mapp-multivariate-analysis-protein-polymorphism
Mutalyzer, https://mutalyzer.nl/
MutationTaster, http://www.mutationtaster.org
PolyPhen-2, http://genetics.bwh.harvard.edu/pph2/
RCSB Protein Data Bank (PDB), http://www.rcsb.org/pdb/home/home.do
RefSeq, https://www.ncbi.nlm.nih.gov/refseq/
SIFT, http://sift.jcvi.org

## References

1. Forgac, M. (2007). Vacuolar ATPases: rotary proton pumps in physiology and pathophysiology. Nat. Rev. Mol. Cell Biol. *8*, 917–929.

2. Cotter, K., Stransky, L., McGuire, C., and Forgac, M. (2015). Recent Insights into the Structure, Regulation, and Function of the V-ATPases. Trends Biochem. Sci. *40*, 611–622.
3. Guillard, M., Dimopoulou, A., Fischer, B., Morava, E., Lefeber, D.J., Kornak, U., and Wevers, R.A. (2009). Vacuolar H+-ATPase meets glycosylation in patients with cutis laxa. Biochim. Biophys. Acta *1792*, 903–914.
4. Karet, F.E., Finberg, K.E., Nelson, R.D., Nayir, A., Mocan, H., Sanjad, S.A., Rodriguez-Soriano, J., Santos, F., Cremers, C.W.R.J., Di Pietro, A., et al. (1999). Mutations in the gene encoding B1 subunit of H+-ATPase cause renal tubular acidosis with sensorineural deafness. Nat. Genet. *21*, 84–90.
5. Kortüm, F., Caputo, V., Bauer, C.K., Stella, L., Ciolfi, A., Alawi, M., Bocchinfuso, G., Flex, E., Paolacci, S., Dentici, M.L., et al. (2015). Mutations in KCNH1 and ATP6V1B2 cause Zimmermann-Laband syndrome. Nat. Genet. *47*, 661–667.
6. Smith, A.N., Skaug, J., Choate, K.A., Nayir, A., Bakkaloglu, A., Ozen, S., Hulton, S.A., Sanjad, S.A., Al-Sabban, E.A., Lifton, R.P., et al. (2000). Mutations in ATP6N1B, encoding a new kidney vacuolar proton pump 116-kD subunit, cause recessive distal renal tubular acidosis with preserved hearing. Nat. Genet. *26*, 71–75.
7. Frattini, A., Orchard, P.J., Sobacchi, C., Giliani, S., Abinun, M., Mattsson, J.P., Keeling, D.J., Andersson, A.K., Wallbrandt, P., Zecca, L., et al. (2000). Defects in TCIRG1 subunit of the vacuolar proton pump are responsible for a subset of human autosomal recessive osteopetrosis. Nat. Genet. *25*, 343–346.
8. Kornak, U., Reynders, E., Dimopoulou, A., van Reeuwijk, J., Fischer, B., Rajab, A., Budde, B., Nürnberg, P., Foulquier, F., Lefeber, D., et al.; ARCL Debré-type Study Group (2008). Impaired glycosylation and cutis laxa caused by mutations in the vesicular H+-ATPase subunit ATP6V0A2. Nat. Genet. *40*, 32–34.
9. Hucthagowder, V., Morava, E., Kornak, U., Lefeber, D.J., Fischer, B., Dimopoulou, A., Aldinger, A., Choi, J., Davis, E.C., Abuelo, D.N., et al. (2009). Loss-of-function mutations in ATP6V0A2 impair vesicular trafficking, tropoelastin secretion and cell survival. Hum. Mol. Genet. *18*, 2149–2165.
10. Mohamed, M., Kouwenberg, D., Gardeitchik, T., Kornak, U., Wevers, R.A., and Morava, E. (2011). Metabolic cutis laxa syndromes. J. Inherit. Metab. Dis. *34*, 907–916.
11. Vanakker, O., Callewaert, B., Malfait, F., and Coucke, P. (2015). The Genetics of Soft Connective Tissue Disorders. Annu. Rev. Genomics Hum. Genet. *16*, 229–255.
12. Adzhubei, I.A., Schmidt, S., Peshkin, L., Ramensky, V.E., Gerasimova, A., Bork, P., Kondrashov, A.S., and Sunyaev, S.R. (2010). A method and server for predicting damaging missense mutations. Nat. Methods *7*, 248–249.
13. Kumar, P., Henikoff, S., and Ng, P.C. (2009). Predicting the effects of coding non-synonymous variants on protein function using the SIFT algorithm. Nat. Protoc. *4*, 1073–1081.
14. Schwarz, J.M., Cooper, D.N., Schuelke, M., and Seelow, D. (2014). MutationTaster2: mutation prediction for the deep-sequencing age. Nat. Methods *11*, 361–362.
15. Tavtigian, S.V., Deffenbaugh, A.M., Yin, L., Judkins, T., Scholl, T., Samollow, P.B., de Silva, D., Zharkikh, A., and Thomas, A. (2006). Comprehensive statistical study of 452 BRCA1 missense substitutions with classification of eight recurrent substitutions as neutral. J. Med. Genet. *43*, 295–305.
16. Mathe, E., Olivier, M., Kato, S., Ishioka, C., Hainaut, P., and Tavtigian, S.V. (2006). Computational approaches for predicting the biological effect of p53 missense mutations: a comparison of three sequence analysis based methods. Nucleic Acids Res. *34*, 1317–1325.
17. Stone, E.A., and Sidow, A. (2005). Physicochemical constraint violation by missense substitutions mediates impairment of protein function and disease severity. Genome Res. *15*, 978–986.
18. Lek, M., Karczewski, K.J., Minikel, E.V., Samocha, K.E., Banks, E., Fennell, T., O'Donnell-Luria, A.H., Ware, J.S., Hill, A.J., Cummings, B.B., et al.; Exome Aggregation Consortium (2016). Analysis of protein-coding genetic variation in 60,706 humans. Nature *536*, 285–291.
19. Wildeman, M., van Ophuizen, E., den Dunnen, J.T., and Taschner, P.E. (2008). Improving sequence variant descriptions in mutation databases and literature using the Mutalyzer sequence variation nomenclature checker. Hum. Mutat. *29*, 6–13.
20. Zhang, Y. (2008). I-TASSER server for protein 3D structure prediction. BMC Bioinformatics *9*, 40.
21. Roy, A., Kucukural, A., and Zhang, Y. (2010). I-TASSER: a unified platform for automated protein structure and function prediction. Nat. Protoc. *5*, 725–738.
22. Yang, J., Yan, R., Roy, A., Xu, D., Poisson, J., and Zhang, Y. (2015). The I-TASSER Suite: protein structure and function prediction. Nat. Methods *12*, 7–8.
23. Zhao, J., Benlekbir, S., and Rubinstein, J.L. (2015). Electron cryomicroscopy observation of rotational states in a eukaryotic V-ATPase. Nature *521*, 241–245.
24. Pettersen, E.F., Goddard, T.D., Huang, C.C., Couch, G.S., Greenblatt, D.M., Meng, E.C., and Ferrin, T.E. (2004). UCSF Chimera–a visualization system for exploratory research and analysis. J. Comput. Chem. *25*, 1605–1612.
25. Dunbrack, R.L., Jr. (2002). Rotamer libraries in the 21st century. Curr. Opin. Struct. Biol. *12*, 431–440.
26. Heide, H., Bleier, L., Steger, M., Ackermann, J., Dröse, S., Schwamb, B., Zörnig, M., Reichert, A.S., Koch, I., Wittig, I., and Brandt, U. (2012). Complexome profiling identifies TMEM126B as a component of the mitochondrial complex I assembly complex. Cell Metab. *16*, 538–549.
27. Huynen, M.A., Mühlmeister, M., Gotthardt, K., Guerrero-Castillo, S., and Brandt, U. (2016). Evolution and structural organization of the mitochondrial contact site (MICOS) complex and the mitochondrial intermembrane space bridging (MIB) complex. Biochim. Biophys. Acta *1863*, 91–101.
28. Bai, X., Zhou, D., Brown, J.R., Crawford, B.E., Hennet, T., and Esko, J.D. (2001). Biosynthesis of the linkage region of glycosaminoglycans: cloning and activity of galactosyltransferase II, the sixth member of the beta 1,3-galactosyltransferase family (beta 3GalT6). J. Biol. Chem. *276*, 48189–48195.
29. Nakajima, M., Mizumoto, S., Miyake, N., Kogawa, R., Iida, A., Ito, H., Kitoh, H., Hirayama, A., Mitsubuchi, H., Miyazaki, O., et al. (2013). Mutations in B3GALT6, which encodes a glycosaminoglycan linker region enzyme, cause a spectrum of skeletal and connective tissue disorders. Am. J. Hum. Genet. *92*, 927–934.
30. Malfait, F., Kariminejad, A., Van Damme, T., Gauche, C., Syx, D., Merhi-Soussi, F., Gulberti, S., Symoens, S., Vanhauwaert, S., Willaert, A., et al. (2013). Defective initiation of glycosaminoglycan synthesis due to B3GALT6 mutations causes a pleiotropic Ehlers-Danlos-syndrome-like connective tissue disorder. Am. J. Hum. Genet. *92*, 935–945.
31. Schindelin, J., Arganda-Carreras, I., Frise, E., Kaynig, V., Longair, M., Pietzsch, T., Preibisch, S., Rueden, C., Saalfeld, S.,

Schmid, B., et al. (2012). Fiji: an open-source platform for biological-image analysis. Nat. Methods *9*, 676–682.
32. Schindelin, J., Rueden, C.T., Hiner, M.C., and Eliceiri, K.W. (2015). The ImageJ ecosystem: An open platform for biomedical image analysis. Mol. Reprod. Dev. *82*, 518–529.
33. Schneider, C.A., Rasband, W.S., and Eliceiri, K.W. (2012). NIH Image to ImageJ: 25 years of image analysis. Nat. Methods *9*, 671–675.
34. Alazami, A.M., Al-Qattan, S.M., Faqeih, E., Alhashem, A., Alshammari, M., Alzahrani, F., Al-Dosari, M.S., Patel, N., Alsagheir, A., Binabbas, B., et al. (2016). Expanding the clinical and genetic heterogeneity of hereditary disorders of connective tissue. Hum. Genet. *135*, 525–540.
35. He, P., Ng, B.G., Losfeld, M.-E., Zhu, W., and Freeze, H.H. (2012). Identification of intercellular cell adhesion molecule 1 (ICAM-1) as a hypoglycosylation marker in congenital disorders of glycosylation cells. J. Biol. Chem. *287*, 18210–18217.
36. Fischer, B., Dimopoulou, A., Egerer, J., Gardeitchik, T., Kidd, A., Jost, D., Kayserili, H., Alanay, Y., Tantcheva-Poor, I., Mangold, E., et al. (2012). Further characterization of ATP6V0A2-related autosomal recessive cutis laxa. Hum. Genet. *131*, 1761–1773.
37. Morava, E., Guillard, M., Lefeber, D.J., and Wevers, R.A. (2009). Autosomal recessive cutis laxa syndrome revisited. Eur. J. Hum. Genet. *17*, 1099–1110.
38. Sun-Wada, G.-H., Imai-Senga, Y., Yamamoto, A., Murata, Y., Hirata, T., Wada, Y., and Futai, M. (2002). A proton pump ATPase with testis-specific E1-subunit isoform required for acrosome acidification. J. Biol. Chem. *277*, 18098–18105.
39. Jansen, J.C., Cirak, S., van Scherpenzeel, M., Timal, S., Reunert, J., Rust, S., Pérez, B., Vicogne, D., Krawitz, P., Wada, Y., et al. (2016). CCDC115 Deficiency Causes a Disorder of Golgi Homeostasis with Abnormal Protein Glycosylation. Am. J. Hum. Genet. *98*, 310–321.
40. Jansen, J.C., Timal, S., van Scherpenzeel, M., Michelakakis, H., Vicogne, D., Ashikov, A., Moraitou, M., Hoischen, A., Huijben, K., Steenbergen, G., et al. (2016). TMEM199 Deficiency Is a Disorder of Golgi Homeostasis Characterized by Elevated Aminotransferases, Alkaline Phosphatase, and Cholesterol and Abnormal Glycosylation. Am. J. Hum. Genet. *98*, 322–330.
41. Ramachandran, N., Munteanu, I., Wang, P., Ruggieri, A., Rilstone, J.J., Israelian, N., Naranian, T., Paroutis, P., Guo, R., Ren, Z.-P., et al. (2013). VMA21 deficiency prevents vacuolar ATPase assembly and causes autophagic vacuolar myopathy. Acta Neuropathol. *125*, 439–457.
42. Jansen, E.J.R., Timal, S., Ryan, M., Ashikov, A., van Scherpenzeel, M., Graham, L.A., Mandel, H., Hoischen, A., Iancu, T.C., Raymond, K., et al. (2016). ATP6AP1 deficiency causes an immunodeficiency with hepatopathy, cognitive impairment and abnormal protein glycosylation. Nat. Commun. *7*, 11600.
43. van Scherpenzeel, M., Steenbergen, G., Morava, E., Wevers, R.A., and Lefeber, D.J. (2015). High-resolution mass spectrometry glycoprofiling of intact transferrin for diagnosis and subtype identification in the congenital disorders of glycosylation. Transl. Res. *166*, 639–649.e1.
44. Mauvezin, C., Nagy, P., Juhász, G., and Neufeld, T.P. (2015). Autophagosome-lysosome fusion is independent of V-ATPase-mediated acidification. Nat. Commun. *6*, 7007.
45. Hucthagowder, V., Sausgruber, N., Kim, K.H., Angle, B., Marmorstein, L.Y., and Urban, Z. (2006). Fibulin-4: a novel gene for an autosomal recessive cutis laxa syndrome. Am. J. Hum. Genet. *78*, 1075–1080.

**The American Journal of Human Genetics, Volume *100***

## Supplemental Data

# Mutations in *ATP6V1E1* or *ATP6V1A* Cause Autosomal-Recessive Cutis Laxa

**Tim Van Damme, Thatjana Gardeitchik, Miski Mohamed, Sergio Guerrero-Castillo, Peter Freisinger, Brecht Guillemyn, Ariana Kariminejad, Daisy Dalloyaux, Sanne van Kraaij, Dirk J. Lefeber, Delfien Syx, Wouter Steyaert, Riet De Rycke, Alexander Hoischen, Erik-Jan Kamsteeg, Sunnie Y. Wong, Monique van Scherpenzeel, Payman Jamali, Ulrich Brandt, Leo Nijtmans, G. Christoph Korenke, Brian H.Y. Chung, Christopher C.Y. Mak, Ingrid Hausser, Uwe Kornak, Björn Fischer-Zirnsak, Tim M. Strom, Thomas Meitinger, Yasemin Alanay, Gulen E. Utine, Peter K.C. Leung, Siavash Ghaderi-Sohi, Paul Coucke, Sofie Symoens, Anne De Paepe, Christian Thiel, Tobias B. Haack, Fransiska Malfait, Eva Morava, Bert Callewaert, and Ron A. Wevers**

**Supplemental Note. Case Reports**

Family I

PI:1 was born as the first child of healthy first cousin Iranian parents. She was born at 39 weeks of gestation after an uneventful pregnancy and normal vaginal delivery. Birth weight (3700 grams), length (52 cm) and occipitofrontal circumference (OFC; 36 cm) were all within normal range. She had severe and generalized cutis laxa, and presented with multiple dysmorphic features including a triangular and progeroid face, a short forehead, overfolded ear helices, hypertelorism, entropion, a prominent beaked nose, a broad nasal tip and columella with narrow nostrils, a long philtrum, an open mouth and a short and pointed chin. Additional features included hypotonia, clenched hands, ulnar deviation of the fingers, congenital hip dysplasia (Graf type 4 on ultrasound), flexion contractures of the knees and club feet. Echocardiography showed a severe dilatation of the ascending aortic root and mild to moderate biventricular hypertrophy. Abdominal ultrasound was normal. She passed away at the age of four months.

First trimester ultrasound in a second pregnancy showed increased nuchal thickness and cardiac abnormalities, but karyotyping of amniocytes was normal (46, XX). The pregnancy was terminated at 21 weeks of gestation. The female fetus (PI:2) had a low weight for gestational age, hypertelorism, low-set ears, increased nuchal thickness and a right hypoplastic heart syndrome with a small and hypoplastic right ventricle, tricuspid valve stenosis and a hypoplastic pulmonary artery.

Family II

PII:1 is a 10-year-old Kuwaiti girl and the first child of a second degree, double consanguineous couple. She was born at term (37 + 2/7 weeks) with a normal birth weight (3430 grams). Shortly after birth she developed severe respiratory insufficiency secondary to bilateral pneumothorax. Her skin was very wrinkled with excessive skin folds and she also presented with bilateral entropion and hip dysplasia. The entropion was surgically corrected at the age of five months and she had surgery for the hip dysplasia at the age of 18 months. She was last seen by a clinical geneticist at the age of ten years and seven months. She suffered from disabling muscular hypotonia and was unable to climb stairs or walk long distances. Clinical examination showed an alert, lean and slender girl. Body length and weight were 134 cm ($3^{rd}$ - $10^{th}$ percentile) and 23.5 kg (below $3^{rd}$ percentile), respectively. Her skin was wrinkled with some excessive skin folds, but not fragile. She had mild scoliosis, pedes planovalgi, hypermobile joints and marked muscular atrophy. Her facial gestalt was characterized by a long and triangular face, overfolded ear helices, hypertelorism, deepset eyes, discrete nystagmus, a broad and high nasal root, dental crowding, a highly arched palate, prominent nasolabial folds and a short and pointed chin. Intelligence was normal. Echocardiography at the age of ten years showed mild dilatation of the right ventricle in the absence of pulmonary hypertension, an atrial septal defect, mitral valve prolapse with grade I-II mitral insufficiency, grade I aortic and tricuspid insufficiency and reduced diastolic compliance, but no cardiomyopathy or aortic dilatation. ECG showed an incomplete right bundle branch block. Cerebral MRI at the ages of two and eight years and abdominal ultrasound

at the age of ten years were all normal. An X-ray of the left hand showed an age-appropriate bone age, undermineralization, overgrowth of the ulnar styloid processus, mild hypertubulation of the phalanges and sharp demarcation of their metaphyseal endplates. Laboratory results showed normal blood count, kidney function, electrolytes and hemostasis, but increased AST (109 U/L, reference value: 11-50 U/l), ALT (71 U/l, 7-31 U/l), LDH (367 U/l, 143-290 U/l), alkaline phosphatase (765 U/l, 69-325 U/l) and creatine kinase (532 U/l, 36-219 U/l; CK). Plasma concentrations of phenylalanine and tyrosine were normal. An extended neurometabolic screening using tandem mass spectrometry was unremarkable.

Her brother (PII:2) presented with a very similar phenotype. He was born with cutis laxa, scoliosis, laryngomalacia, entropion, bilateral cryptorchidism, bilateral inguinal hernias and bilateral pneumothorax. At the age of seven and eight years, he had rodding surgery to correct a progressive scoliosis. He had severe muscle hypoplasia, preventing him from walking distances over 500 m or climbing stairs. His intelligence was normal. At the age of nine and a half years he measured 122 cm (below 3$^{rd}$ percentile) and weighed 18.6 kg (below 3$^{rd}$ percentile). He had a slender habitus, very soft and excessive skin, very little subcutaneous fat, prominent muscle hypoplasia and severely reduced muscle force. He also presented with a pronounced dextroconvex scoliosis, chest deformity and pedes plani. His facial appearance was remarkable due to a triangular face, hypertelorism, entropion, nystagmus, overfolded ear helices, a beaked and prominent nose with a high nasal root and broad nasal tip and columella, and narrow nostrils, prominent nasolabial folds, a short and pointed chin, an open mouth, a highly arched palate, malpositioned teeth and temporomandibular joint dysfunction with recurrent dislocations. Echocardiography and abdominal ultrasound were normal. An X-ray of the left hand showed an age-appropriate bone age, undermineralization, sharp delineation of the metaphyses and overgrowth of the ulnar styloid processus with delayed ossification and mild flaring of the ulnar epiphysis. Routine biochemical analysis revealed elevated serum levels of AST (86 U/l, 11-50 U/l), ALT (59 U/l, 7-40 U/l), LDH (351 U/l, 143-290 U/l), CK (426 U/l, 36-219 U/l) and alkaline phosphatase (549 U/l, 86-315 U/l). The plasma concentration of glycine was slightly elevated, but phenylalanine and tyrosine concentrations were normal. Urinary amino acid and organic acid concentrations were normal and homocystinuria was excluded. An extended neurometabolic screening using tandem mass spectrometry was unremarkable.

Family III

PIII:1 was born as the first child of non-consanguineous German parents. His clinical phenotype was reported earlier.[1] In summary, he was referred for metabolic and genetic work-up because of severe neonatal cutis laxa and an abnormal serum glycosylation pattern (Table S3). In addition, he presented with dysmorphic facial features, including downslanting palpebral fissures, large and prominent ears, bilateral cataract, an abnormal fat distribution and hypotonia. He failed to thrive with postnatal growth restriction and a microcephaly. Cerebral MRI showed enlarged ventricles with white matter involvement and periventricular parieto-occipital gliosis. He has a developmental delay affecting both

cognitive and motor performance. At the age of four years he developed hypertrophic cardiomyopathy, which has remained stable. He was last evaluated at the age of 14 years. He was normocephalic (25$^{th}$ percentile), and body length and weight were on the 75$^{th}$ percentile and 50$^{th}$ percentile, respectively. The severe, inelastic, generalized sagging skin improved over time, but no improvement occurred in the lipodystrophy. A few months later, he suffered a generalized tonic-clonic seizure.

Family IV

PIV:1 was born as the third child of healthy, consanguineous parents of Pakistani descent. His two older sisters were healthy. Prenatal ultrasound showed bilateral cerebral ventriculomegaly, a ventricular septal defect and overriding aorta. After a spontaneous delivery, he had an irregular breathing pattern and required respiratory support. His birth weight (3745 grams) was within normal limits. His skin was lax and wrinkled. He had hypotonia and reduced spontaneous leg movements. Multiple dysmorphic features were present: he had a bulbous nose with a broad nasal bridge, simple folded auricles and a receding chin. There was a suspicion of a submucosal cleft palate. In addition, he presented with severe bilateral club feet, dislocation of the hips, flexion contractures of all joints, camptodactyly and bilateral simian creases. He had a micropenis, cryptorchidism and a right inguinal hernia. Echocardiography showed a small atrial septal defect and a dilated ascending aorta with a tortuous aortic arch. The neonatal course was further complicated by progressive cardiac failure, pneumonia, sepsis and a 36 misnute resuscitation following dislocation of an endotracheal tube. Shortly after birth, he developed epileptic seizures, which evolved to generalized and complex partial seizures at the age of two months. Initial EEGs showed a burst suppression pattern, which later evolved to hypsarrhythmia. Cerebral MRI revealed diffuse thickening of the cerebral cortex, most prominent in frontal lobes and was suggestive of polymicrogyria. The myelination pattern was abnormal and the corpus callosum thin. A basic metabolic screen did not show any abnormalities. The child passed away after a long period of intensive treatments.

Family V

This male child (PV:1) was born to consanguineous parents of Turkish descent. Laxity of the skin with extensive folding was noted at birth. He had a triangular face with hypertelorism, blepharophimosis, entropion, a bulbous nose and a small receding chin. Cardiac ultrasound revealed a ventricular septal defect. MRI brain showed an anatomic variant of the cavum septum pellucidum. Ophthalmologic evaluation revealed paucity of the optic disk. He was not hypotonic, but CK levels were increased.

**Figure S1. Clinical phenotype of PI:2 (termination at 21 weeks of gestation)**

**Figure S2. Tissue-specific Gene Expression of V-ATPase Subunits**

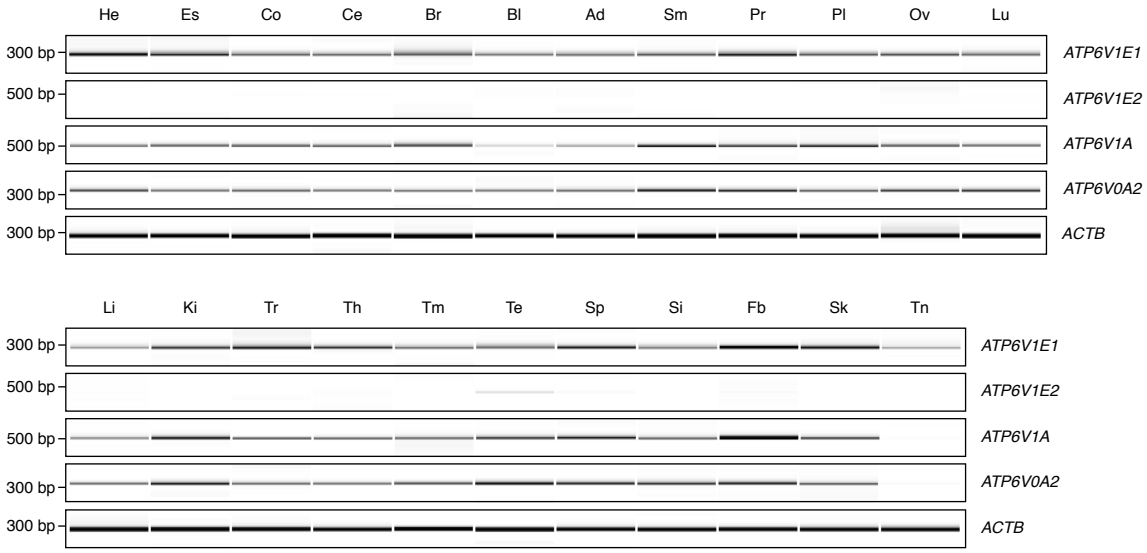


Tissue-specific expression of *ATP6V1E1*, *ATP6V1E2*, *ATP6V1A* and *ATP6V0A2* was assessed using the FirstChoice Human Total RNA Survey Panel (Life Technologies), human tendon (OriGene) and adult skin RNA (BioGenomics) and pooled RNA from three human dermal fibroblast cultures. cDNA was synthesized with the iScript cDNA Synthesis kit (Bio-Rad Laboratories). For each gene of interest, reverse transcription PCR (RT-PCR) was performed using two primer pairs (only one is shown) and an aliquot of each reaction was analyzed on the Caliper LabChip GX (Caliper Life Sciences). *ACTB* was included as loading control. The darker the bands the higher the expression of the gene of interest in a tissue. RT-PCR showed ubiquitous expression of *ATP6V1E1*, *ATP6V1A* and *ATP6V0A2*. The expression of *ATP6V1E2* was restricted to testicular tissue. Abbreviations are as follows: bp, base pairs; He, heart; Es, esophagus; Co, colon; Ce, cervix; Br, brain; Bl, bladder; Ad, adipose; Sm, skeletal muscle; Pr, prostate; Pl, placenta; Ov, ovary; Lu, lung; Li, liver; Ki, kidney; Tr, trachea; Th, thyroid; Tm, thymus; Te, testes; Sp, spleen; Si, small intestine; Fb, fibroblasts; Sk, skin; Tn, tendon.

**Figure S3. Quadrupole-Time-of-Flight Mass Spectrometry of Intact Transferrin**

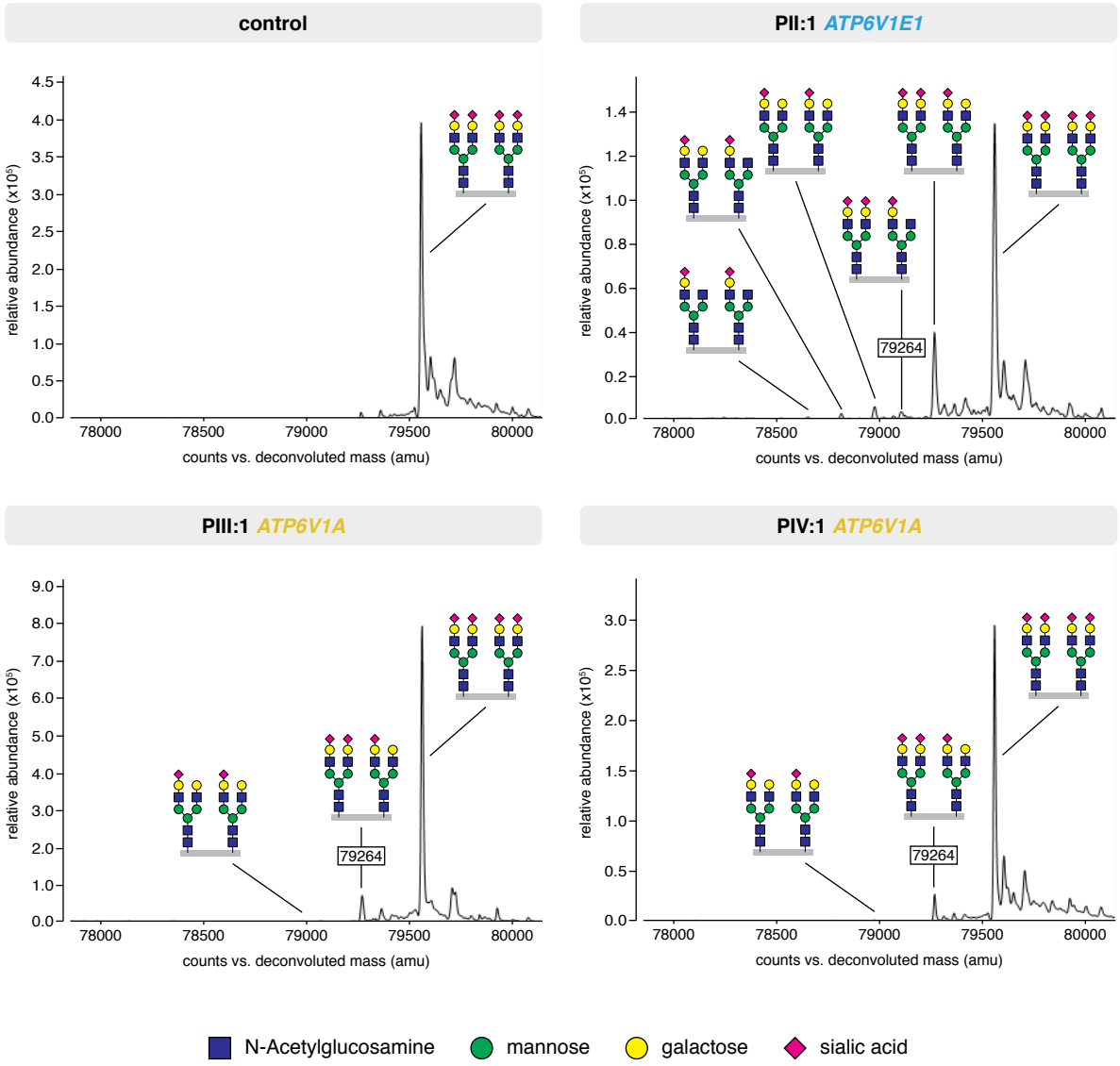


Quadrupole-time-of-flight (Q-TOF) mass spectrometry (MS) of intact transferrin showed a consistent increase of mass 79264 in all evaluated affected individuals (PII:1, at age 10; PIII:1, at age 13; PIV:1, before the age of 1), corresponding to the loss of one sialic acid. In addition, a minor lack of galactose was observed in Family II (PII:1).

**Table S1. V-ATPase Subunits Identified by Complexome Profiling**

| subunit | gene | GI accession # | annotation | $M_r$ (kDa) | peptides | sequence coverage (%) |
|---|---|---|---|---|---|---|
| **$V_1$ cytosolic domain** | | | | | | |
| A | *ATP6V1A* | 19913424 | V-type proton ATPase subunit A | 68.303 | 40 | 83 |
| B2 | *ATP6V1B2* | 19913428 | V-type proton ATPase subunit B, isoform 2 | 56.500 | 27 | 69 |
| C1 | *ATP6V1C1* | 4502315 | V-type proton ATPase subunit C, isoform 1 | 43.941 | 25 | 65 |
| D1 | *ATP6V1D* | 7706757 | V-type proton ATPase subunit D | 28.262 | 14 | 57 |
| E1 | *ATP6V1E1* | 4502317 | V-type proton ATPase subunit E, isoform 1 | 26.145 | 15 | 58 |
| F | *ATP6V1F* | 20357547 | V-type proton ATPase subunit F, isoform 1 | 13.370 | 6 | 68 |
| G1 | *ATP6V1G1* | 4757818 | V-type proton ATPase subunit G, isoform 1 | 13.757 | 9 | 75 |
| H | *ATP6V1H* | 47717100 | V-type proton ATPase subunit H, isoform 2 | 54.151 | 12 | 34 |
| **$V_0$ transmembrane domain** | | | | | | |
| a1 | *ATP6V0A1* | 19913418 | V-type proton ATPase subunit a, isoform 1 | 95.755 | 34 | 44 |
| a2 | *ATP6V0A2* | 42741679 | V-type proton ATPase subunit a, isoform 2 | 98.081 | 15 | 22 |
| a3 | *TCIRG1* | 19924145 | V-type proton ATPase subunit a, isoform 3 | 92.967 | 35 | 53 |
| c | *ATP6V0C* | 4502313 | V-type proton ATPase subunit c | 15.736 | 2 | 32 |
| d1 | *ATP6V0D1* | 19913432 | V-type proton ATPase subunit d, isoform 1 | 40.329 | 18 | 54 |
| **accessory subunits** | | | | | | |
| Ac45 | *ATP6AP1* | 17136148 | V-type proton ATPase subunit S1 precursor | 52.025 | 18 | 40 |
| M8-9 | *ATP6AP2* | 15011918 | renin receptor precursor | 39.008 | 13 | 42 |

**Table S2. *In Silico* Prediction of Pathogenicity for Missense Variants**

| | cDNA | protein | PolyPhen-2 | SIFT | MutationTaster | Align GVGD | MAPP |
|---|---|---|---|---|---|---|---|
| ***ATP6V1E1*** | c.383T>C | p.Leu128Pro | probably damaging | deleterious | disease causing | C0 | bad |
| | c.634C>T | p.Arg212Trp | probably damaging | deleterious | disease causing | C0 | bad |
| ***ATP6V1A*** | c.1012C>T | p. Arg338Cys | probably damaging | deleterious | disease causing | C0 | bad |
| | c.215G>A | p.Gly72Asp | probably damaging | deleterious | disease causing | C65 | bad |

The following reference sequences were used: *ATP6V1E1* (MIM: 108746; GenBank: NM_001696.3) and *ATP6V1A* (MIM: 607027; GenBank: NM_001690.3). Abbreviations are as follows: PolyPhen-2, Polymorphism Phenotyping v2; MAPP, Multivariate Analysis of Protein Polymorphism.

**Table S3. Glycosylation Screening**

| | age | transferrin isofocusing | | | | | | ApoCIII isofocusing | | | | | | MS |
|---|---|---|---|---|---|---|---|---|---|---|---|---|---|---|
| | | disialo | | trisialo | | tetrasialo | | ApoCIII-0 | | ApoCIII-1 | | ApoCIII-2 | | |
| | years | value (%) | ref. (%) | value (%) | ref. (%) | value (%) | ref. (%) | value (%) | ref. (%) | value (%) | ref. (%) | value (%) | ref. (%) | value (%) |
| **PII:1** | 10 | **14.4 ↑** | 3.3 – 7.6 | **28.9 ↑** | 4.9 – 0.6 | **32.2 ↓** | 47.3 – 62.7 | **8.7** | 0 – 11.6 | **50.2** | 33.1 – 66.9 | **41.1** | 27.4 – 60.0 | **29.3 ↑** |
| **PII:2** | 9 | **12.9 ↑** | 3.3 – 7.6 | **29.6 ↑** | 4.9 – 10.6 | **35.4 ↓** | 47.3 – 62.7 | **13.1 ↑** | 0 – 11.6 | **55.1** | 33.1 – 66.9 | **31.7** | 27.4 – 60.0 | **27.4 ↑** |
| **PIII:1** | 6 | **3.6** | 3.3 – 7.6 | **12.9 ↑** | 4.9 – 10.6 | **62.5** | 47.3 – 62.7 | **NA** | | **NA** | | **NA** | | **9.1 ↑** |
| | 7 | **5.7** | 3.3 – 7.6 | **15.9 ↑** | 4.9 – 10.6 | **50.2** | 47.3 – 62.7 | **8.1** | 0 – 11.6 | **57.9** | 33.1 – 66.9 | **34.0** | 27.4 – 60.0 | **15.9 ↑** |
| | 13 | **3.2 ↓** | 3.3 – 7.6 | **11.8 ↑** | 4.9 – 10.6 | **71.0 ↑** | 47.3 – 62.7 | **5.4** | 0 – 11.6 | **70.2 ↑** | 33.1 – 66.9 | **24.4 ↓** | 27.4 – 60 | **14.9 ↑** |
| **PIV:1** | <1 | **3.6** | 3.3 – 7.6 | **11.0 ↑** | 4.9 – 10.6 | **62.1** | 47.3 – 62.7 | **2.6** | 0.2 – 4.5 | **40.9 ↓** | 42.7 – 69.9 | **56.5** | 26.2 – 56.7 | **9.2 ↑** |

Quantification of transferrin and apolipoprotein CIII (ApoCIII) isoelectric focusing and the loss of sialic acid on quadrupole-time-of-flight (Q-TOF) mass spectrometry (MS) analysis represented as relative abundance of the main peak of the normal tetrasialic transferrin (ref. 3.5 ± 1.9%). Abbreviations are as follows: NA, not available; ref., reference value.

**Supplemental References**

1. Van Asbeck, E., Wolthuis, D.F.G.J., Mohamed, M., Wevers, R.A., Korenke, C.G., Gardeitchik, T., and Morava, E. (2014). A novel phenotype associated with cutis laxa, abnormal fat distribution, cardiomyopathy and cataract. Am. J. Med. Genet. A *164A*, 1049–1055.